Initiation of a Proto-Transform Fault Prior to Seafloor Spreading

F. Illsley-Kemp[1,2], J. M. Bull[1], D. Keir[1,3], T. Gerya[4], C. Pagli[5], T. Gernon[1], A. Ayele[6], B. Goitom[7], J. O. S. Hammond[8], and J. M. Kendall[7].

Finnigan Illsley-Kemp, finnigan.illsleykemp@vuw.ac.nz

[1]National Oceanography Centre Southampton, University of Southampton, Southampton, United Kingdom

[2]School of Geography, Environment and Earth Sciences, Victoria University of Wellington, Wellington, New Zealand

[3]Dipartimento di Scienze della Terra, Università degli Studi di Firenze, Florence, Italy

[4]Institute of Geophysics, ETH Zürich, Zürich, Switzerland

[5]Dipartimento di Scienze della Terra, Università di Pisa, Pisa, Italy

This article has been accepted for publication and undergone full peer review but has not been through the copyediting, typesetting, pagination and proofreading process, which may lead to differences between this version and the Version of Record. Please cite this article as doi: 10.1029/2018GC007947

Abstract. Transform faults are a fundamental tenet of plate tectonics, connecting offset extensional segments of mid-ocean ridges in ocean basins worldwide. The current consensus is that oceanic transform faults initiate after the onset of seafloor spreading. However, this inference has been difficult to test given the lack of direct observations of transform fault formation. Here, we integrate evidence from surface faults, geodetic measurements, local seismicity, and numerical modelling of the subaerial Afar continental rift and show that a proto-transform fault is initiating during the final stages of continental breakup. This is the first direct observation of proto-transform fault initiation in a continental rift, and sheds unprecedented light on their formation mechanisms. We demonstrate that they can initiate during late-stage continental rifting, earlier in the rifting cycle than previously thought.

[6]Institute of Geophysics Space Science
and Astronomy, Addis Ababa University,
Addis Ababa, Ethiopia

[7]School of Earth Sciences, University of
Bristol, Bristol, United Kingdom

[8]Institute of Geophysics Space Science
and Astronomy, Addis Ababa University,
Addis Ababa, Ethiopia

Future studies of volcanic rifted margins cannot assume that oceanic transform faults initiated after the onset of seafloor spreading.

Keypoints:

- We document the initiation of a proto-transform fault during late stage continental rifting in Afar, Ethiopia.
- Surface faulting, seismicity and geodetic observations reveal extensional transfer between magmatic segments.
- Numerical modelling predicts that the region between the offset magmatic segments will evolve to a stable oceanic transform fault.

1. Introduction

Transform faults have long been known to play a key role in seafloor spreading (Macdonald et al., 1988). They link and accommodate strike-slip motion between laterally offset mid-ocean ridge segments, and occur in ocean basins worldwide. Despite the prevalence of oceanic transform faults, their initiation has not been directly observed and thus their formation mechanisms are poorly understood. Oceanic transform faults rely heavily on strain accommodation by magmatism and are orthogonal to spreading segments and parallel to the spreading direction (Taylor, Goodliffe, Martiniez, & Hey, 1995). In contrast, extension in early-stage continental rifts is controlled by slip on overlapping, en-echelon normal faults (Ebinger, 1989). Where these faults overlap, they are linked by oblique accommodation zones (Ebinger, 1989 ; Bosworth, Lister, Ethington, & Symonds, 1986). Previous numerical modelling of continental rifting has suggested that oceanic-style transform faults do not form in early-stage rifts (Allken, Huismans, & Thieulot, 2012), so it is generally assumed that transform faults originate during seafloor spreading (Eagles, Pérez-Díaz, & Scarselli, 2015 ; Nguyen, Hall, Bird, & Ball, 2016). However, it is not known whether transform fault can initiate in mature continental rift systems.

The geometric correspondence between mid-ocean ridges and the segmentation of passive margins has led some studies to propose that some large-scale fracture zones have structural inheritance from the late stages of continental rifting (Cochran & Martinez, 1988 ; McClay & Khalil, 1998 ; Behn & Lin, 2000). In contrast, many studies suggest that short-scale transform faults are not inherited from continental rift geometry and the majority of transform faults show no clear evidence of structural inheritance (Bosworth

et al., 1986 ; Taylor et al., 1995 ; Taylor, Goodliffe, & Martinez, 2009). The Danakil region, in northern Afar, Ethiopia/Eritrea, is one of the few areas on Earth where the final stages of continental rifting are subaerially exposed (Figure 1). The region thus provides a unique opportunity to explore the timing of transform fault initiation, and to understand the kinematics of their formation.

1.1. Continental Rifting in Northern Afar

In Afar, the southern extent of the Red Sea rift steps on-land into the Afar depression (McClusky et al., 2010) (Figure 1). The crust thins from ∼27 km in the central and southern Afar rift, to <15 km beneath the Danakil region in the north (Hammond et al., 2011 ; Makris & Ginzburg, 1987). However, the crust in the Danakil region is still significantly thicker than that commonly observed in the oceans (White, McKenzie, & O'Nions, 1992), which, together with its seismic velocity structure (Hammond et al., 2011 ; Makris & Ginzburg, 1987), suggests it is thinned and heavily intruded continental crust. The marked thinning of the crust into the Danakil region has been attributed to a late stage of plate weakening and stretching caused by protracted and localized magma intrusion (Bastow & Keir, 2011). Since the Quaternary, strain in Afar has localized to axial magmatic segments, hypothesized to be the future boundary of continental breakup (Hayward & Ebinger, 1996), and is thought to be accommodated through magmatic intrusions and associated mechanical faulting (Barberi & Varet, 1977 ; Wolfenden, Ebinger, Yirgu, Renne, & Kelley, 2005 ; Manighetti et al., 2001). (Illsley-Kemp et al., 2018) have shown that the majority of seismicity and extension is focused at the rift-axis, which steps en-echelon to the Northeast from the Dabbahu magmatic segment. However, a signifi-

cant amount of seismicity occurs at the western rift margin, in a complex set of marginal grabens (Figure 1).

In the Danakil region, two currently active magmatic spreading segments, the Erta-Ale and Tat-Ale segments, separate the Nubian plate from the Danakil microplate (Figure 1). The Erta-Ale magmatic segment consists of 12 volcanic centres, including Erta-Ale volcano with its persistent lava lake (Keir, Bastow, Pagli, & Chambers, 2013). To the south, offset laterally by ∼20 km to the east is the Tat-Ale magmatic centre. The Giulietti Plain lies in the offset region between the Erta-Ale and Tat-Ale magmatic segments (Figure 3). The plain is below sea level and is predominantly overlain by evaporites from repeated marine incursions (Keir et al., 2013) and contains the saline Lake Afrera. Acoustic bathymetric profiles from the lake reveal Red Sea parallel normal faults intersected by oblique structures. These structures have been compared to those responsible for nodal deeps at oceanic transforms (Bonatti et al., 2017). Extension rates in the Danakil region are analogous to ultraslow/slow spreading ridges (Dick & Schouten, 2003) varying from ∼7 mm yr^{-1} in the north (15°N) to ∼20 mm yr^{-1} in the south (13°N). Extension is orientated 058°, roughly perpendicular to the spreading segment axes (McClusky et al., 2010).

2. Observational Methods and Results

2.1. Structural Geology

Surface faults were mapped remotely using Google Earth (DigitalGlobe) and ArcGIS. The surface expression of faults was mapped and digitized to create a detailed fault map (Figure 2). The strike of the faults was approximated using the start and end points of each mapped fault. Strike distributions are weighted according to fault length and displayed in 10° binned rose diagrams (Figure 2).

Analysis of the mapped surface faults (>2000 faults) demonstrates that mean orientations within the Erta-Ale (157°±14°) and Tat-Ale (145°±8°) segments are consistent with the direction of maximum extension, which is approximately 058° (McClusky et al., 2010). In addition, these segments exhibit low variation in fault orientations, whereas surface faults in the Giulietti Plain show greater variability (147°±28°) (Figure 2). While we must consider the possibility that not all of these surface faults are tectonic in origin (Eusden, Dykstra, Pettinga, & Campbell, 2005), we interpret the increased variability in fault orientations in the Giulietti Plain as being due to interaction between the Erta-Ale and Tat-Ale magmatic segments. The increased variability may also be evidence for an immature, evolving fault zone (Hatem, Cooke, & Toeneboehn, 2017).

2.2. Seismicity

A network of 20 seismometers in both Ethiopia and Eritrea (Figure 1) provided continuous seismic data for two years between February 2011 and February 2013. A total of 4971 earthquakes of magnitude 0.4–5.8 were recorded during the experiment and were located with a 2-D velocity model (Hammond et al., 2011 ; Makris & Ginzburg, 1987 ; Lomax, Virieux, Volant, & Berge-Thierry, 2000). These earthquakes have average location errors of ±1.9 km and ±4.1 km in the horizontal and vertical directions respectively, and the catalogue is complete above magnitude 2.0 (Illsley-Kemp, Keir, et al., 2017). Generally, earthquakes are focused at the western rift margin, which separates the Ethiopian plateau from the Afar depression, or in the vicinity of volcanic centres (Illsley-Kemp et al., 2018) (Figure 1). In addition, there is a cluster of 418 earthquakes focused within the Giulietti Plain, at the region of observed horizontal strain and fault interaction (Figure 1).

We relocate the seismicity within the Giulietti Plain using GrowClust (Trugman & Shearer, 2017) (Figure 3a), a technique which develops upon the double-difference relocation method (Waldhauser & Ellsworth, 2000). This process increases the relative location accuracy for clustered earthquakes. Initial average location errors were markedly improved for relocated events, which have an average relative hypocentral error of ±0.55 km. The majority of the relocated earthquakes occur in the upper 5 km of the crust. Focal mechanisms were calculated for three clusters of relocated earthquakes using the polarities of the first P and S-wave arrivals and the software FocMec (Snoke, 2003). The resultant focal mechanisms display a characteristic right lateral strike slip motion with a component of extension (Figure 3b). The nodal plane is inferred from surface faults resulting in a mean strike and dip of 135°±9° and 75°±7° respectively.

2.3. Satellite Geodesy

We combine an extensive set of InSAR from multiple tracks and GPS measurements (Figure S1) to invert for the three-dimensional velocity and strain field of Afar, following a two-step approach (Pagli, Wang, Wright, Calais, & Lewi, 2014). We obtained maps of the line of sight (LOS) average surface velocities for each InSAR track using a multi-interferogram method (Wang & Wright, 2012) and then we combined these with the GPS velocities using a velocity-field method (Kogan et al., 2012). The LOS interferograms were created using images from the Envisat satellite in both descending and ascending orbits, in image and wide-swath modes, spanning the period between 2007 and 2010 (Pagli et al., 2014). GPS sites in central Afar were measured between 2007 and 2010 (Kogan et al., 2012), while GPS velocities from the Red Sea coast, the Gulf of Aden, and the Main Ethiopian rift are from other sources (McClusky et al., 2010 ; Kogan et al., 2012 ; Saria,

Calais, Stamps, Delvaux, & Hartnady, 2014 ; Vigny, Huchon, Ruegg, Khanbari, & Asfaw, 2006 ; Vigny et al., 2007). All GPS velocities were combined in the common International Terrestrial Reference Frame 2008 and given with respect to a stationary Nubian plate. Sudden deformations, induced by eruptions and dyke intrusions in Afar, were subtracted from the GPS as well as the InSAR data as they may affect the strain-field in the Giulietti Plain (Pagli et al., 2014). No sudden deformations were removed from the Giulietti Plain, therefore the strain field in our study area is complete.

To invert for the continuous three-dimensional velocity field we divided the Afar region into a mesh of triangular elements (Figure S1) and assumed that the velocity varies linearly within each triangle (Pagli et al., 2014). The geodetic observations (InSAR and GPS) within each triangle are related to the velocities of their vertices by an interpolation function. We inverted for the velocities of the triangular vertices using the system of equations described by (Nooner et al., 2009). The system was solved using a least square method that included full variance-covariance matrices as well as smoothing with a Laplacian operator. A smoothing factor that minimizes the trade-off between the solution roughness and the weighted RMS misfit of the model was selected (Pagli et al., 2014). After finding the velocities at the vertices of the triangles, we calculate the horizontal strain rates at each vertex using spherical approximation equations (Savage, Gan, & Svarc, 2001).

We find a region of elevated maximum horizontal shear strain rate (up to 4×10^{-7} yr^{-1}) concentrated between the Tat-Ale and Erta-Ale segments, with the maximum shear strain rate to the west of the Tat-Ale segment (Figure 3c). No sudden discrete or large magnitude deformation has occurred in the vicinity of the Giulietti Plain during this period, and

therefore we interpret the strain rates as representative of the tectonic regime. These geodetic results show that active shear is occurring in the Giulietti Plain.

2.4. Summary of Observations

The strike slip events show excellent correlation with the observed region of maximum shear strain rate (Figure 3c). In addition our focal mechanisms are consistent with the orientations of principal strain rate axes, which suggest right lateral strike slip faults on planes generally trending NW-SE (Figure 4). The surface faults in the Giuletti Plain have a range of orientations, from ∼NW-SE to ∼N-S (Figure 2), the strike of the focal mechanisms (135°) aligns with the most NW-SE of these surface faults. This suggests that the NW-SE oriented surface faults are active in the present day. By extension, this suggests that the ∼N-S oriented surface faults were active in the past but are inactive now. Therefore, the orientation of faulting within the Giulietti Plain has rotated in an anticlockwise direction through time. The combination of earthquake locations, focal mechanisms, surface faulting trends and geodetic strain rates, imply that the right lateral strike slip events are accommodating oblique shear between the two magmatic segments. In this way, extension is transferred between the two magmatic segments.

3. Thermomechanical Numerical Modelling

The nucleation and evolution of oceanic transform faults has been the subject of several analogue and numerical modelling studies (Gerya, 2012). Analog freezing wax experiments (O'Bryan, Cohen, & Gilliland, 1975) reproduced features indicative of seafloor spreading, including transform faults and inactive fracture zones. These studies showed that the spreading-parallel pattern of transform faults is an intrinsically preferential orientation.

With the advent of high-powered computing, studies involving complex three-dimensional numerical models have begun to investigate transform fault formation. Such numerical studies (Hieronymus, 2004 ; Choi, Lavier, & Gurnis, 2008 ; Gerya, 2013b), suggest that crustal thinning is promoted in the region of the transform fault at low to intermediate spreading rates. In addition, these studies suggest that transform faults can form at initially straight ridges which become unstable due to asymmetric crustal accretion. This leads to the formation of a new transform fault and suggests that they are not necessarily inherited from offsets in the initial rift (Gerya, 2010a, 2010b).

To investigate the temporal evolution of this extension transfer in the Giulietti Plain we use high-resolution 3D thermomechanical numerical models that simulate the extensional setting in the Danakil region. The Eulerian-Lagrangian visco-plastic model with an internal free surface allows for large strains and spontaneous crustal growth by magmatic accretion. The employed numerical technique (Gerya, 2010a, 2010b, 2013b) is based on a combination of a finite difference method applied on a uniformly spaced staggered finite difference grid, with the marker-in-cell technique. Full details of the numerical modelling are given in (Gerya, 2013b).

The initial model setup corresponds to late stage continental rifting in Northern Afar, with a 20 km thick crust (Figure S3). Similarly to previous numerical models of spontaneous plate fragmentation (Gerya, 2013b ; Hieronymus, 2004 ; Choi et al., 2008), two linear thermal perturbations (weak seeds) with an offset of 20–40 km are imposed at the bottom of the lithospheric mantle. The modelled (full) spreading rate corresponds to 20 mm yr^{-1}, taken from GPS studies in the region (McClusky et al., 2010). The numeri-

cal model thus simulates the final stages of continental rifting, where the crust has been significantly modified by repeated magmatic intrusions, such as in Afar.

The momentum, mass and heat conservation equations are solved with the thermomechanical code I3ELVIS (Gerya & Yuen, 2007) on the non-deforming Eulerian grid, whereas the advection of transport properties including viscosity, plastic strain, temperature etc. is performed by advecting the Lagrangian markers. We adopted the tectono-magmatic numerical model of rifting and spreading developed by (Gerya, 2013b), which accounts for the four key physical processes: (i) thermal accretion of the oceanic mantle lithosphere resulting in plate thickness growth, (ii) partial melting of the asthenospheric mantle, melt extraction and percolation toward the ridge resulting in crustal growth, (iii) magmatic accretion of the new crust under the ridge and (iv) hydrothermal circulation at the axis of the ridge, resulting in excess cooling of the crust. These physical processes are included in our numerical model in a simplified manner.

Thermal accretion of the mantle lithosphere is modelled by solving the heat conduction equation combined with a temperature-dependent viscosity for the non-molten mantle (Katz, Spiegelman, & Langmuir, 2003). Consequently, cooling causes asthenospheric mantle to become rheologically strong and accrete spontaneously to the bottom of the lithosphere. Hydrothermal circulation at the axis of the ridge, producing rapid cooling of the new crust (Theissen-Krah, Iyer, Rüpke, & Morgan, 2011), is parameterized with an enhanced thermal conductivity of the crust in the regions located below sea level (Gregg, Behn, Lin, & Grove, 2009). The hydrothermal circulation in the crust is controlled by the Nusselt number, which we range between 1–2 (Gerya, 2013b) and find that it has little effect on model evolution. Partial melting of the asthenospheric mantle, melt extraction

and percolation toward the ridge is implemented in a simplified manner. According to our model, crustal growth at the ridge is balanced by the melt production and extraction in the mantle. However, melt percolation toward the ridge (Katz, 2010) is not modelled directly and considered to be nearly instantaneous (Connolly, Schmidt, Solferino, & Bagdassarov, 2009). Lagrangian markers track the amount of melt extracted during the evolution of each experiment. Magmatic accretion of the new crust is modelled by spontaneous cooling and crystallization of melts at the walls of the lower-crustal magma regions (Wanless & Shaw, 2012).

The rheological response to elastic strain in the mantle and crust is controlled by the upper strain limit for fracture-related weakening (γ_0). The Eulerian computational domain is equivalent to $98 \times 98 \times 50$ km and is resolved with a regular rectangular grid of $197 \times 197 \times 101$ nodes and contains 34 million randomly distributed Lagrangian markers. We performed 16 numerical experiments (Table S1) by systematically varying different model parameters in their uncertainty ranges. Here we describe the evolution of the reference model *afab*.

3.1. Modelling Results

During the initial stages of the model, offset rift grabens form above the thermal perturbations (Figure 6a). At 0.9 Myr into the model, two volcanic ridges form at the centre of the two grabens as a result of decompression melting of the rising asthenosphere. At this stage of the model new oceanic style crust begins to form at the volcanic centres through the crystallization of melt at the walls of the magmatic regions (Figure 6). The model does not attempt to simulate small scale intrusions, thus this formation of oceanic style crust may be analogous to the intrusion of dykes and sills, commonly observed in

the Danakil region. Initially these volcanic ridges are separated by ∼80 km in the along strike direction. As the model develops the ridges propagate towards each other such that by 1.8 Myr they are separated along strike by ∼40 km and laterally by ∼20 km (Figure b), broadly the same configuration as the Erta-Ale and Tat-Ale segments in the Danakil region (Figure 3a). At this stage the volcanic centres begin to interact and form a narrow region of maximum horizontal shear-strain that is orientated ∼27° to the trend of the volcanic ridges and has shear-strain rates of $\sim 10^{-6}$–10^{-5} per year, which is of a similar magnitude to the observed maximum horizontal shear-strain (Figure 3c). This stage of the model can be considered to represent the emergence of a proto-transform fault (Figure b). The angle of the proto-transform fault with respect to the volcanic ridges closely matches the angle between the average strike of earthquakes within the Giulietti Plain and the Erta-Ale segment (Figure 3b).

The model predicts that the deformation within the proto-transform fault is transtensional. This deformation would manifest itself as oblique strike-slip earthquakes in the upper crust, as is observed in the Giulietti Plain (Figure 3b). The extensional component of the proto-transform fault promotes opening and volcanism at the end of each volcanic segment, causing the segments to propagate towards each other (Figure). The proto-transform fault continually reconnects to the propagating segment tips, such that it undergoes an anti-clockwise rotation towards a spreading parallel orientation (Figure c). Evidence for this anti-clockwise rotation of deformation is shown in the surface faults of the Giulietti Plain (Figure 3a).

As the model further develops (∼2.8 Myr), the lithosphere in the proto-transform fault region is predicted to remain continental in composition and acts as a 'bridge' maintaining

a connection between the two plates (Figure 6c). The model then predicts that, at ∼3.8 Myr a transform fault will form between the volcanic segments (Figures d). At this stage deformation on the transform fault is purely strike-slip. These transform faults are then stable features that are persistent in the model as it develops into a mature ridge-transform pattern which closely resembles young, seafloor spreading segments (Taylor et al., 1995). Therefore, our results also suggest that once transform faults have initiated they are stable, persistent features that focus deformation during the transition from continental rifting to seafloor spreading; and that they will continue through to the mature oceanic ridge stage of plate tectonics.

4. Discussion

The mode of extensional transfer in the Giulietti Plain is not observed in early-stage continental rifts. In these less developed rifts, extension is focused along asymmetric half graben structures, and transferred through complex, oblique accommodation zones (Rosendahl, 1987 ; Bosworth et al., 1986 ; Ebinger, 1989 ; Corti, 2008) (Figure 7a). These regions are extremely structurally complex and are dominated by oblque-slip normal faults which strike sub-parallel to the rift (Bosworth et al., 1986). In analogue models of oblique rifting in the Main Ethiopian rift (Corti, 2008 ; Agostini, Corti, Zeoli, & Mulugeta, 2009 ; Corti, Philippon, Sani, Keir, & Kidane, 2013), offset rift segments are connected by a region of strike-slip deformation very similar to what we observe in northern Afar. Conversely, these models predict that the accommodation zone will rotate in line with the sense of strike-slip motion. However, they do not account for the segment propagation which is shown to play a key role in the rotation of the proto-transform fault towards a spreading parallel orientation (Figure 7e). It may be that the regions of strike-slip

deformation observed in the Main Ethiopian Rift are pre-cursors to proto-transform fault initiation.

Where ocean ridge segments overlap by several kilometres, a variety of mechanisms for the transfer of extension have been observed. In Iceland, shear motion between overlapping magmatic segments is shown to occur through bookshelf faulting. (Green, White, & Greenfield, 2014) detail how a region of focused seismicity between the Askja and Kverkfjöll segments is accommodating right-lateral shear motion. This occurs through strike-slip motion along a system of left-lateral faults which are sub-parallel to the magmatic segments (Figure 7b). The bookshelf faulting mode of extensional transfer is therefore fundamentally different to observations from the Giulietti plain as the orientation of slip is opposite, and the active faulting in the Giulietti plain is oblique to the magmatic segments (Figure 3).

Another style of non-transform ocean ridge discontinuity is found where magmatic segment overlap by 10s of kilometres. This results in a focused region of rotational deformation which results in a volcanically active, elevated terrain (Macdonald & Fox, 1983 ; Tyler, Bull, Parson, & Tuckwell, 2007) (Figure 7c). This central domain is the focus for shear and rotational deformation and is thought to be unstable with time. (Macdonald & Fox, 1983) use analogue models of spreading processes to suggest that the overlapping spreading segments will link, leading to the abandonment of the deformation zone. In contrast to previous examples, ocean ridge segments are often arranged en-echelon, with characteristic, ridge-perpendicular oceanic transform faults (Behn & Lin, 2000) (Figure 7f). A mode of extension transfer that is analogous to that currently observed in the Danakil region, and oceanic transform faults, is seen in small-scale faults in bedrock

(Willemse, Peacock, & Aydin, 1997) (Figure 7d). In this setting, shear zones form en-echelon veins which are connected by a system of perpendicular to oblique solution seams. Extensional strain is transferred between veins through displacement along these solution seams.

Similar proto-transform fault systems (Figure 7e) have been observed in young seafloor spreading segments in the Woodlark Basin, Papua New Guinea (Taylor et al., 1995). These systems have been postulated to mark the initiation of transform faults yet are observed only in regions of young seafloor spreading. In addition, a similar mechanism of interacting, propagating magmatic rifts has been proposed for the formation of hyper-extended margins such as those observed in the South Atlantic (Le Pourhiet, May, Huille, Watremez, & Leroy, 2017). The Danakil region is therefore the first observed example of extension transferring between axial magmatic segments through a region of oblique shear, prior to the initiation of seafloor spreading.

Previous studies on transform fault formation do not consider axial localization of strain during continental breakup. However, observations and models of continental rifts increasingly show that as extension increases, faulting and magmatism become focused in-rift to a narrow swath of dense faulting, volcanic centers, and aligned cones with subsurface dykes (Hayward & Ebinger, 1996 ; Manighetti et al., 2001 ; Kendall, Stuart, Ebinger, Bastow, & Keir, 2005 ; Buck, 2006). The border faults that controlled the architecture of the young rift become less active as extension is focused at the rift axis (Hayward & Ebinger, 1996 ; Ebinger & Casey, 2001 ; Wolfenden et al., 2005). In terms of deformation mechanisms this mode of continental rifting is more closely analogous to seafloor spreading than early stage continental rifting. In addition, the mechanisms of magmatic crustal

accretion that have been observed at mid-ocean ridges (Carbotte et al., 2013), have initiated in the Danakil region (Illsley-Kemp et al., 2018). Thus, the transition from late-stage continental rifting to seafloor spreading must be considered as a prolonged process, and processes which are considered indicative of seafloor spreading can initiate prior to final continental breakup.

Considering that the observations from the Danakil region cannot be explained by any previously proposed modes of extensional transfer, the close correspondence between the numerical model and observations provides compelling evidence that the Giulietti Plain is at the proto-transform fault stage of formation. Our results therefore document the direct observation of proto-transform initiation and corroborate previously proposed mechanisms of formation (Gerya, 2013b). The development of the numerical model towards a stable oceanic-style transform fault lends support to the interpretation that the Giulietti Plain is a proto-transform fault. However, we cannot preclude that the Giulietti Plain may develop into a throughgoing, continuous magmatic segment with a zero-offset transform (Schouten & White, 1980) and this behaviour is predicted by model runs with elevated mantle temperatures (Table S1). The transfer of extension between magmatic segments through transform faults is a fundamental characteristic of seafloor spreading (Atwater & Menard, 1970 ; Macdonald et al., 1988). Our results demonstrate, that proto-transform faults can initiate during late stage continental rifting, prior to seafloor spreading (Figure 8). This provides further evidence that seafloor spreading processes can initiate earlier in the rifting cycle than previously thought. During our study period (2011–2013), deformation was focused at the Giulietti Plain, however it is not clear whether this is a long-term pattern. There are many offset magmatic segments in Afar and it is not clear whether the proto-

transform process is limited to the Giulietti Plain. This study focuses on the Giulietti Plain as that is the only segment offset with measurable seismic and geodetic deformation. The lack of measurable deformation between other segment offsets strongly suggests that deformation related to rift linkage is episodic. Other regions of segment offset may have been active in the past and may become active in the future. For example, (Pagli et al., 2014) suggest that the rift axis steps from the Tat-Ale segment to the Dabbahu segment in the SW (Figure 1). The sporadic seismicity in this region may be associated with this transfer of extension, however significant deformation was not observed in this region during our study period.

Rifting in Afar occurs above anomalously hot mantle, which causes significant magma intrusion (Ferguson et al., 2013 ; Gallacher et al., 2016). This magmatism may enable the style of extension in Afar to be more similar to that observed at oceanic ridges (Keir et al., 2013 ; Illsley-Kemp et al., 2018). Studies of the magmatically less active Woodlark basin, Papua New Guinea, which exhibits the transition from continental rift to seafloor spreading, suggest that transform faults initiate as, or after, spreading nucleates (Gerya, 2013a). It is therefore not clear whether our interpretations regarding the timing of transform fault initiation applies beyond the formation of a volcanic rifted margin. However, our research suggests that future work on volcanic rifted margins should not assume that transform faults initiated after the onset of seafloor spreading.

Acknowledgments. We thank SEIS-UK for use of the instruments and their computing facilities. The facilities of SEIS-UK are supported by the Natural Environment Research Council (NERC) under agreement R8/H10/64. FIK is funded through NERC studentship NE/L002531/1, a grant to GSNOCS from Roy Franklin OBE and the ECLIPSE

Programme, funded by the New Zealand Ministry of Business, Innovation and Employment. DK is supported by NERC grant NE/L013932. Funding for fieldwork is from BHP Billiton. TG is supported by NERC grant NE/R004978/1. BG is funded through a PhD scholarship by the University of Bristol and Engineering and Physical Sciences Research Council (EPSRC: Grant Number DTG EP/L504919/1). We also acknowledge assistance from Addis Ababa University and the Afar National Regional State Government. Continuous waveform data is available at the IRIS data repository. Earthquake information is available in the supplementary material of (Illsley-Kemp et al., 2018). Mapped fault data is available in the supplementary information.

Références

Agostini, A., Corti, G., Zeoli, A., & Mulugeta, G. (2009). Evolution, pattern, and partitioning of deformation during oblique continental rifting: Inferences from lithospheric-scale centrifuge models. *Geochem. Geophys. Geosyst.*, *10*(11). 10.1029/2009GC002676

Allken, V., Huismans, R. S., & Thieulot, C. (2012). Factors controlling the mode of rift interaction in brittle-ductile coupled systems: A 3D numerical study. *Geochem. Geophys. Geosyst.*, *13*(5).

Atwater, T., & Menard, H. (1970). Magnetic lineations in the northeast pacific. *Earth Planet. Sci. Lett.*, *7*(5), 445–450.

Barberi, F., & Varet, J. (1977). Volcanism of Afar: Small-scale plate tectonics implications. *Geological Society of America Bulletin*, *88*(9), 1251–1266.

Bastow, I., & Keir, D. (2011). The protracted development of the continent-ocean transition in Afar. *Nat. Geosci.*, *4*, 248-250. 10.1038/NGEO01095

Behn, M. D., & Lin, J. (2000). Segmentation in gravity and magnetic anomalies along the US East Coast passive margin: Implications for incipient structure of the oceanic lithosphere. *J. Geophys. Res.*, *105*(B11), 25769–25790.

Bonatti, E., Gasperini, E., Vigliotti, L., Lupi, L., Vaselli, O., Polonia, A., & Gasperini, L. (2017). Lake Afrera, a structural depression in the Northern Afar Rift (Red Sea). *Heliyon*, *3*(5), e00301.

Bosworth, W., Lister, G., Ethington, R., & Symonds, P. (1986). Comment and reply on Detachment faulting and the evolution of passive continental margins. *Geology*, *14*(10), 890–892.

Buck, W. (2006). The role of magma in the development of the Afro-Arabian Rift System, in The Structure and Evolution of the East African Rift System in the Afar Volcanic Province, eds. Yirgu, G. Ebinger, C.J. & Maguire, P.K.H. *Geol. Soc. Lond. Spec. Pub.*, *259*, 43-54.

Carbotte, S. M., Marjanović, M., Carton, H., Mutter, J. C., Canales, J. P., Nedimović, M. R.Perfit, M. R. (2013). Fine-scale segmentation of the crustal magma reservoir beneath the East Pacific Rise. *Nat. Geosci.*, *6*(10), 866.

Choi, E.-s., Lavier, L., & Gurnis, M. (2008). Thermomechanics of mid-ocean ridge segmentation. *Phys. Earth Planet. Int.*, *171*(1), 374–386.

Cochran, J. R., & Martinez, F. (1988). Evidence from the northern Red Sea on the transition from continental to oceanic rifting. *Tectonophysics*, *153*(1-4), 25–53.

Connolly, J. A., Schmidt, M. W., Solferino, G., & Bagdassarov, N. (2009). Permeability of asthenospheric mantle and melt extraction rates at mid-ocean ridges. *Nature*, *462*(7270), 209–212.

Corti, G. (2008). Control of rift obliquity on the evolution and segmentation of the main Ethiopian rift. *Nat. Geosci.*, *1*(4), 258–262.

Corti, G., Philippon, M., Sani, F., Keir, D., & Kidane, T. (2013). Re-orientation of the extension direction and pure extensional faulting at oblique rift margins: comparison between the Main Ethiopian Rift and laboratory experiments. *Terra Nova*, *25*(5), 396–404.

Dick, H., & Schouten, H. (2003). An ultraslow-spreading class of ocean ridge. *Nature*, *426*, 405-412.

Eagles, G., Pérez-Díaz, L., & Scarselli, N. (2015). Getting over continent ocean boundaries. *Earth-Science Reviews*, *151*, 244–265.

Ebinger, C. J. (1989). Tectonic development of the western branch of the East African rift system. *Geol. Soc. Am. Bull.*, *101*(7), 885–903.

Ebinger, C. J., & Casey, M. (2001). Continental breakup in magmatic provinces: an Ethiopian example. *Geology*, *29*, 527-530.

Eusden, J., Dykstra, J., Pettinga, J. R., & Campbell, J. K. (2005). Structural collapse of a transpressive hanging-wall fault wedge, Charwell region of the Hope fault, South Island, New Zealand. *New Zealand Journal of Geology and Geophysics*, *48*(2), 295–309.

Ferguson, D. J., Maclennan, J., Bastow, I., Pyle, D., Jones, S., Keir, D.Yirgu, G. (2013). Melting during late-stage rifting in Afar is hot and deep. *Nature*, *499*(7456), 70–73.

Gallacher, R. J., Keir, D., Harmon, N., Stuart, G., Leroy, S., Hammond, J. O.others (2016). The initiation of segmented buoyancy-driven melting during continental breakup. *Nat. Comm.*, *7*.

Gerya, T. (2010a). Dynamical instability produces transform faults at mid-ocean ridges. *Science*, *329*(5995), 1047–1050.

Gerya, T. (2010b). *Introduction to numerical geodynamic modelling*. Cambridge University Press.

Gerya, T. (2012). Origin and models of oceanic transform faults. *Tectonophysics*, *522*, 34–54.

Gerya, T. (2013a). Initiation of transform faults at rifted continental margins: 3D petrological-thermomechanical modeling and comparison to the Woodlark Basin. *Petrology*, *21*(6), 550–560.

Gerya, T. (2013b). Three-dimensional thermomechanical modeling of oceanic spreading initiation and evolution. *Phys. Earth Planet. Int.*, *214*, 35–52.

Gerya, T., & Yuen, D. A. (2007). Robust characteristics method for modelling multiphase visco-elasto-plastic thermo-mechanical problems. *Physics of the Earth and Planetary Interiors*, *163*(1), 83–105.

Green, R. G., White, R. S., & Greenfield, T. (2014). Motion in the north Iceland volcanic rift zone accommodated by bookshelf faulting. *Nat. Geosci.*, *7*(1), 29–33.

Gregg, P. M., Behn, M. D., Lin, J., & Grove, T. L. (2009). Melt generation, crystallization, and extraction beneath segmented oceanic transform faults. *J. Geophys. Res.*, *114*(B11).

Hammond, J. O. S., Kendall, J.-M., Stuart, G., Keir, D., Ebinger, C., Ayele, A., & Belachew, M. (2011). The nature of the crust beneath the Afar triple junction: Evidence from receiver functions. *Geochem. Geophys. Geosyst.*, *12*(12).

Hatem, A. E., Cooke, M. L., & Toeneboehn, K. (2017). Strain localization and evolving

kinematic efficiency of initiating strike-slip faults within wet kaolin experiments. *J. Struct. Geol.*, *101*, 96–108.

Hayward, N., & Ebinger, C. (1996). Variations in the along–axis segmentation of the Afar rift system. *Tectonics*, *15*, 244–257.

Hieronymus, C. F. (2004). Control on seafloor spreading geometries by stress-and strain-induced lithospheric weakening. *Earth Planet. Sci. Lett.*, *222*(1), 177–189.

Illsley-Kemp, F., Keir, D., Bull, J. M., Ayele, A., Hammond, J. O., Kendall, J.-M.Goitom, B. (2017). Local earthquake magnitude scale and b-value for the Danakil region of northern Afar. *Bull. Seis. Soc. Am.*, *107*(2), 521–531.

Illsley-Kemp, F., Keir, D., Bull, J. M., Gernon, T. M., Ebinger, C., Ayele, A.others (2018). Seismicity during continental breakup in the Red Sea rift of Northern Afar. *J. Geophys. Res.*, *123*, 2.

Illsley-Kemp, F., Savage, M. K., Keir, D., Hirschberg, H. P., Bull, J. M., Gernon, T. M.Goitom, B. (2017). Extension and stress during continental breakup: Seismic anisotropy of the crust in Northern Afar. *Earth Planet. Sci. Lett.*, *477*, 41–51.

Katz, R. F. (2010). Porosity-driven convection and asymmetry beneath mid-ocean ridges. *Geochem. Geophys. Geosyst.*, *11*(11).

Katz, R. F., Spiegelman, M., & Langmuir, C. H. (2003). A new parameterization of hydrous mantle melting. *Geochem. Geophys. Geosyst.*, *4*(9).

Keir, D., Bastow, I. D., Pagli, C., & Chambers, E. L. (2013). The development of extension and magmatism in the Red Sea rift of Afar. *Tectonophysics*, *607*, 98–114.

Kendall, J.-M., Stuart, G., Ebinger, C., Bastow, I., & Keir, D. (2005). Magma assisted rifting in Ethiopia. *Nature*, *433*, 146-148.

Kogan, L., Fisseha, S., Bendick, R., Reilinger, R., McClusky, S., King, R., & Solomon, T. (2012). Lithospheric strength and strain localization in continental extension from observations of the East African Rift. *J. Geophys. Res.*, *117*(B3).

Le Pourhiet, L., May, D. A., Huille, L., Watremez, L., & Leroy, S. (2017). A genetic link between transform and hyper-extended margins. *Earth Planet. Sci. Lett.*, *465*, 184–192.

Lomax, A., Virieux, J., Volant, P., & Berge-Thierry, C. (2000). Probabilistic earthquake location in 3D and layered models. In *Advances in seismic event location* (pp. 101–134). Springer.

Macdonald, K. C., & Fox, P. (1983). Overlapping spreading centres: New accretion geometry on the East Pacific Rise. *Nature*.

Macdonald, K. C., Fox, P., Perram, L., Eisen, M., Haymon, R., Miller, S.Shor, A. (1988). A new view of the mid-ocean ridge from the behaviour of ridge-axis discontinuities. *Nature*, *335*(6187), 217–225.

Makris, J., & Ginzburg, A. (1987). The Afar Depression: transition between continental rifting and sea floor spreading. *Tectonophysics*, *141*, 199-214.

Manighetti, I., Tapponnier, P., Courtillot, V., Gallet, Y., Jacques, E., & Gillot, P.-Y. (2001). Strain transfer between disconnected, propagating rifts in Afar. *J. Geophys. Res.*, *106*(B7), 13613–13665.

McClay, K., & Khalil, S. (1998). Extensional hard linkages, eastern Gulf of Suez, Egypt. *Geology*, *26*(6), 563–566.

McClusky, S., Reilinger, R., Ogubazghi, G., Amleson, A., Healeb, B., Vernant, P.Kogan, L. (2010). Kinematics of the southern Red Sea–Afar Triple Junction and implications

for plate dynamics. *Geophys. Res. Lett.*, *37*(5).

Nguyen, L. C., Hall, S. A., Bird, D. E., & Ball, P. J. (2016). Reconstruction of the East Africa and Antarctica continental margins. *J. Geophys. Res.*, *121*(6), 4156–4179.

Nooner, S. L., Bennati, L., Calais, E., Buck, W. R., Hamling, I. J., Wright, T. J., & Lewi, E. (2009). Post-rifting relaxation in the Afar region, Ethiopia. *Geophys. Res. Lett.*, *36*(21).

O'Bryan, J., Cohen, R., & Gilliland, W. (1975). Experimental origin of transform faults and straight spreading-center segments. *Geol. Soc. Amer. Spec. Paper*, *86*(6), 793–796.

Pagli, C., Wang, H., Wright, T. J., Calais, E., & Lewi, E. (2014). Current plate boundary deformation of the Afar rift from a 3-D velocity field inversion of InSAR and GPS. *J. Geophys. Res.*, *119*(11), 8562–8575.

Rosendahl, B. R. (1987). Architecture of continental rifts with special reference to East Africa. *Annual Review of Earth and Planetary Sciences*, *15*(1), 445–503.

Saria, E., Calais, E., Stamps, D., Delvaux, D., & Hartnady, C. (2014). Present-day kinematics of the East African Rift. *J. Geophys. Res.*, *119*(4), 3584–3600.

Savage, J., Gan, W., & Svarc, J. (2001). Strain accumulation and rotation in the Eastern California Shear Zone. *J. Geophys. Res.*, *106*(B10), 21995–22007.

Schouten, H., & White, R. S. (1980). Zero-offset fracture zones. *Geology*, *8*(4), 175–179.

Snoke, J. A. (2003). FOCMEC: focal mechanism determinations. *International Handbook of Earthquake and Engineering Seismology*, *85*, 1629–1630.

Taylor, B., Goodliffe, A., & Martinez, F. (2009). Initiation of transform faults at rifted continental margins. *Comptes Rendus Geoscience*, *341*(5), 428–438.

Taylor, B., Goodliffe, A., Martiniez, F., & Hey, R. (1995). Continental rifting and initial sea-floor spreading in the Woodlark Basin. *Nature*, *374*(6522), 534.

Theissen-Krah, S., Iyer, K., Rüpke, L. H., & Morgan, J. P. (2011). Coupled mechanical and hydrothermal modeling of crustal accretion at intermediate to fast spreading ridges. *Earth Planet. Sci. Lett.*, *311*(3), 275–286.

Trugman, D. T., & Shearer, P. M. (2017). GrowClust: A hierarchical clustering algorithm for relative earthquake relocation, with application to the Spanish Springs and Sheldon, Nevada, earthquake sequences. *Seismological Research Letters*, *88*(2A), 379–391.

Tyler, S., Bull, J. M., Parson, L. M., & Tuckwell, G. W. (2007). Numerical modelling of non-transform discontinuity geometry: Implications for ridge structure, volcano-tectonic fabric development and hydrothermal activity at segment ends. *Earth Planet. Sci. Lett.*, *257*(1), 146–159.

Vigny, C., de Chabalier, J.-B., Ruegg, J.-C., Huchon, P., Feigl, K. L., Cattin, R.Kanbari, K. (2007). Twenty-five years of geodetic measurements along the Tadjoura-Asal rift system, Djibouti, East Africa. *J. Geophys. Res.*, *112*(B6).

Vigny, C., Huchon, P., Ruegg, J.-C., Khanbari, K., & Asfaw, L. M. (2006). Confirmation of Arabia plate slow motion by new GPS data in Yemen. *J. Geophys. Res.*, *111*(B2).

Waldhauser, F., & Ellsworth, W. L. (2000). A double-difference earthquake location algorithm: Method and application to the northern Hayward fault, California. *Bull. Seis. Soc. Am.*, *90*(6), 1353–1368.

Wang, H., & Wright, T. (2012). Satellite geodetic imaging reveals internal deformation of western Tibet. *Geophys. Res. Lett.*, *39*(7).

Wanless, V. D., & Shaw, A. M. (2012). Lower crustal crystallization and melt evolution at mid-ocean ridges. *Nat. Geosci.*, *5*(9), 651–655.

White, R. S., McKenzie, D., & O'Nions, R. K. (1992). Oceanic crustal thickness from seismic measurements and rare earth element inversions. *J. Geophys. Res.*, *97*(B13), 19683–19715.

Willemse, E. J., Peacock, D. C., & Aydin, A. (1997). Nucleation and growth of strike-slip faults in limestones from Somerset, UK. *J. Struct. Geol.*, *19*(12), 1461–1477.

Wolfenden, E., Ebinger, C., Yirgu, G., Renne, P., & Kelley, S. (2005). Evolution of a volcanic rifted margin: Southern Red Sea, Ethiopia. *Bull. Geol. Soc. Am.*, *117*(7-8), 846-864.

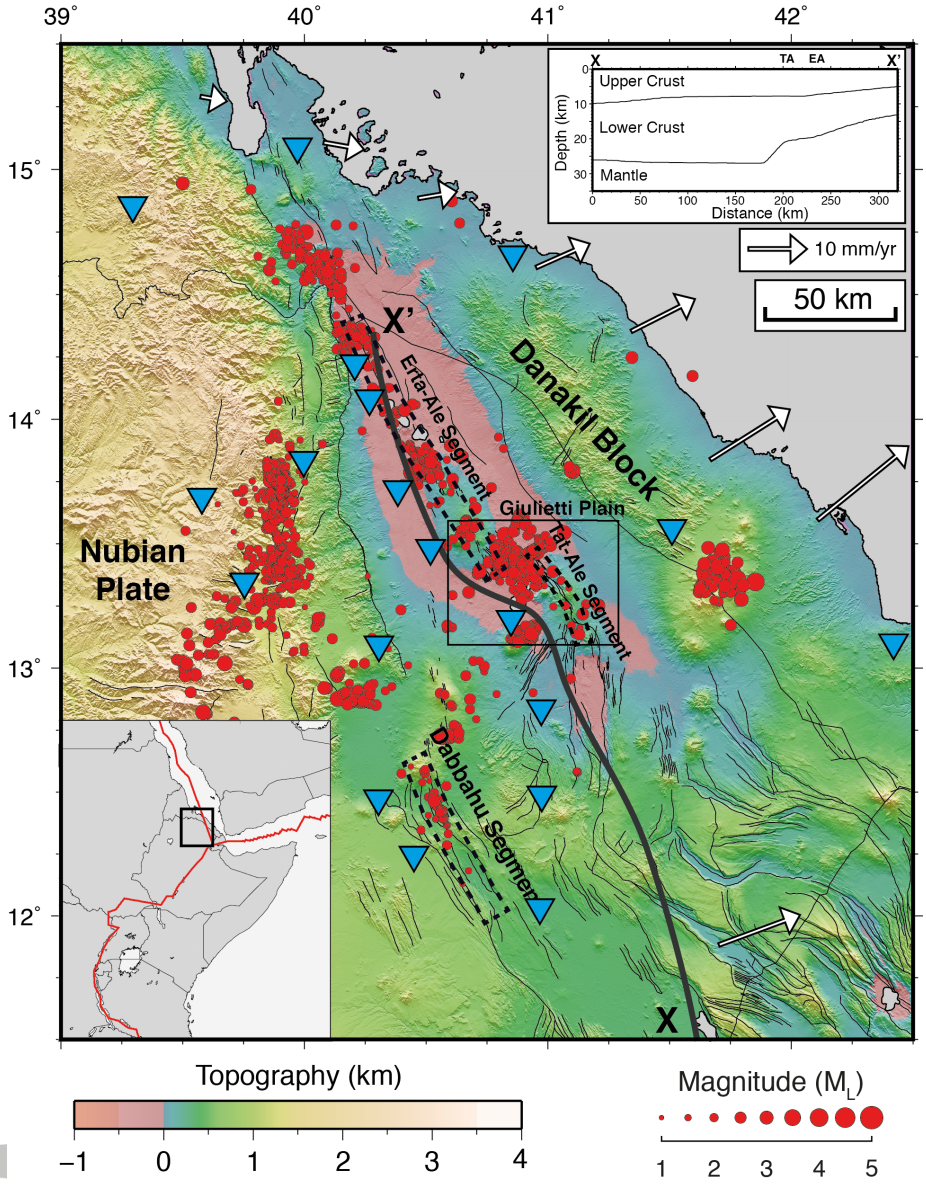

Figure 1. Main figure shows the location of the seismic network (blue inverted triangles) and all recorded earthquakes with horizontal errors <5 km (red circles) from 2011–2013 (Illsley-Kemp et al., 2018), superimposed on topography taken from the Shuttle Radar Topography Mission (SRTM). A cluster of events is located in the Giulietti Plain, between the offset Erta-Ale and Tat-Ale segments. The box encloses the area shown in Figures 2, 3, 4. White arrows denote GPS velocities, relative to a stationary Nubian plate (McClusky et al., 2010). Surface faults shown in black taken from (Manighetti et al., 2001) and (Illsley-Kemp, Savage, et al., 2017). Cross section X–X' marks the seismic refraction profile of (Makris & Ginzburg, 1987), showing thinned crust (<20 km) beneath the Giulietti Plain. Inset shows the location of the Danakil region in East Africa.

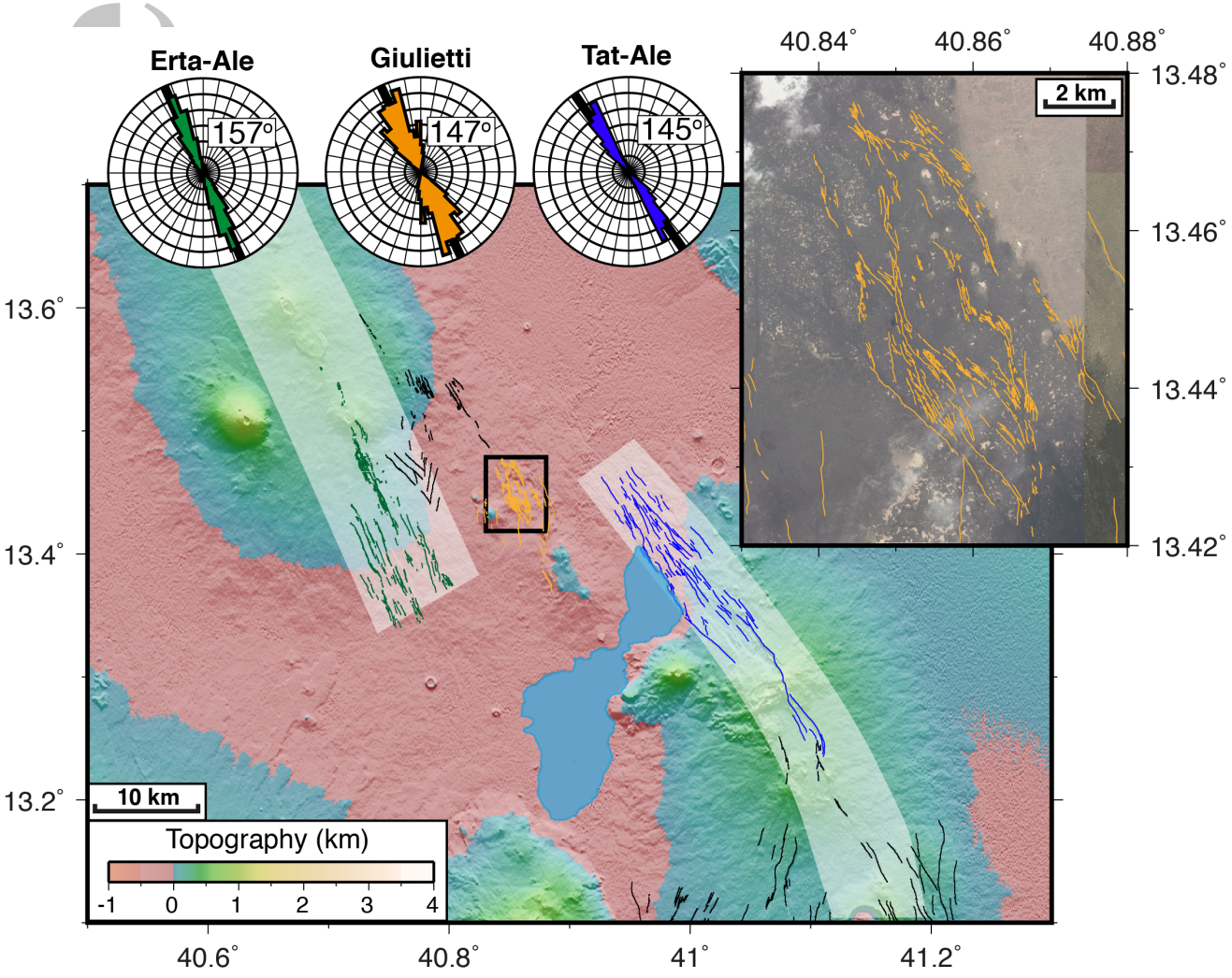

Figure 2. Surface faults and their associated rose diagrams show mean orientations that are consistent with regional extension in the Erta-Ale (green rose diagram) and Tat-Ale (blue rose diagram) segments. However, within the Giulietti Plain (orange rose diagram) surface faults display a greater variation, consistent with an interaction between the two spreading segments. Inset shows a zoom of the Giulietti Plain faults overlain on satellite imagery (Google Earth).

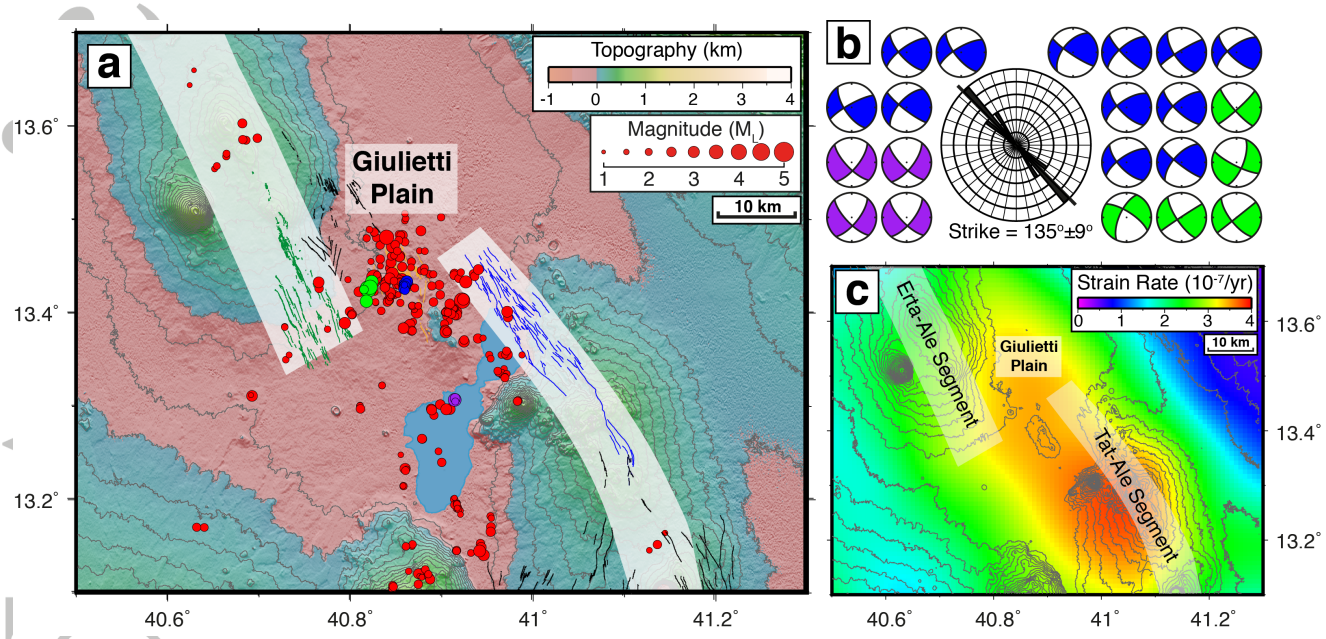

Figure 3. **a)** Relocated earthquakes with average location error of ±0.55 km highlight a clear zone of deformation. **b)** Focal mechanisms for three clusters (colour coded in a) display characteristic right-lateral, oblique strike slip motion. **c)** InSAR and GPS derived maximum horizontal shear strain rate clearly showing a region of high strain rate within the Giulietti Plain. The combination of observations from the Giulietti Plain indicates that extension is transferred between the spreading segments through oblique shear.

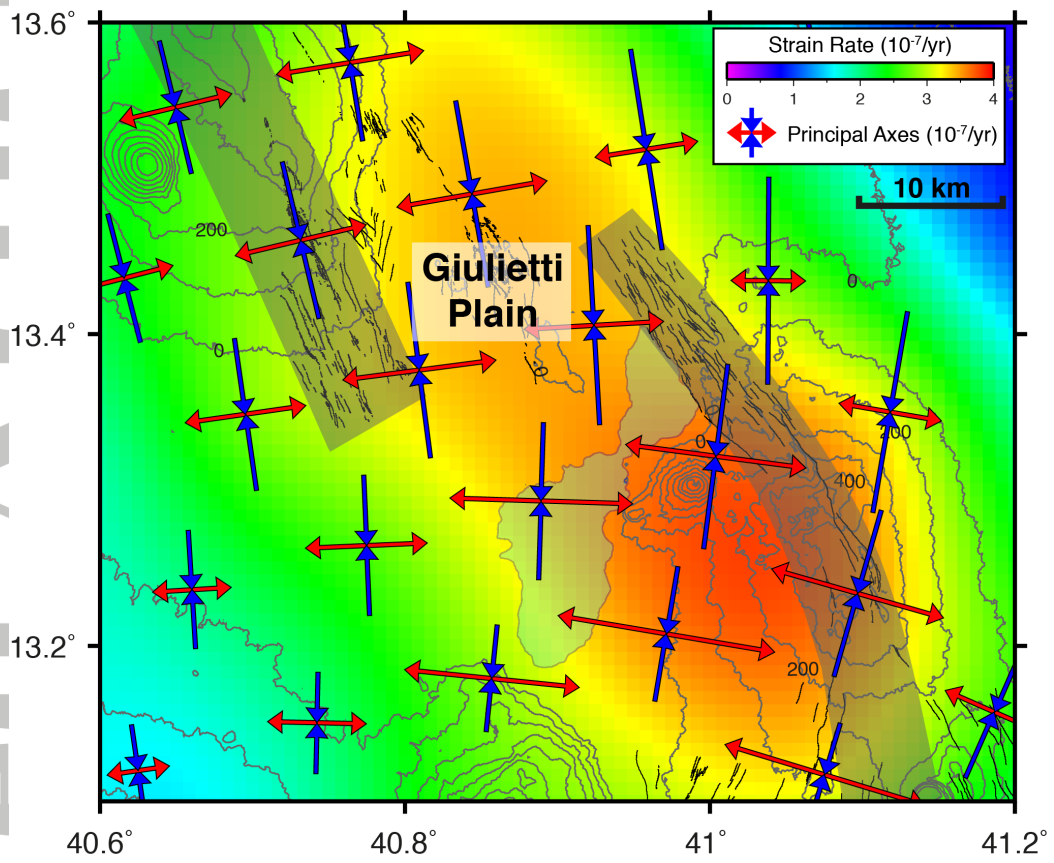

Figure 4. The principal axes of observed maximum horizontal shear strain rates in the Giulietti Plain, from InSAR and GPS data. Extensional (red) and compressional (blue) principal axes of the strain rates, plotted on the maximum shear strain rate. Axes are consistent with right-lateral strike-slip on NW-SE fault planes within the Giulietti plain, in agreement with observed seismicity (Figure 3).

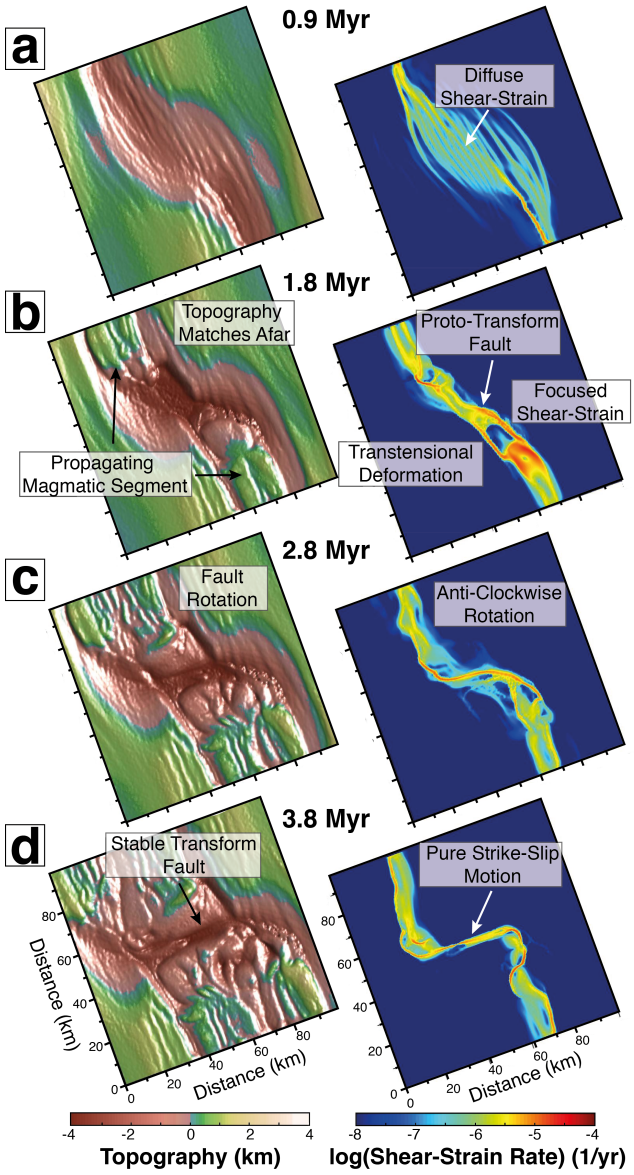

Figure 5. Time steps refer to time after model initiation. Topography (pink below sea level) and horizontal shear-strain rate (at depth of 5 km) initially show a diffuse distribution of shear-strain. This shear-strain develops into a narrow region of transform oblique shear-strain at ~1.8 Myr **(b)** and acts as a proto-transform fault. The topography and ~27° angle between proto-transform fault and volcanic segment closely resemble the topography and strike of earthquakes in Afar. In addition the modelled horizontal shear-strain is of a similar magnitude to that observed in the Giulietti Plain (Figure 3c). The model predicts that the proto-transform fault is transtensional, which would produce oblique strike slip earthquakes, as seen in the Giulietti Plain. The proto-transform fault then rotates **(c)** towards a spreading parallel orientation, this would produce and anticlockwise rotation of surface faults as seen in the Giulietti Plain. At 3.8 Myr **(d)**, the proto-transform fault becomes a stable, spreading parallel transform fault, which separates the two magmatic segments and is a persistent feature for the remaining model time.

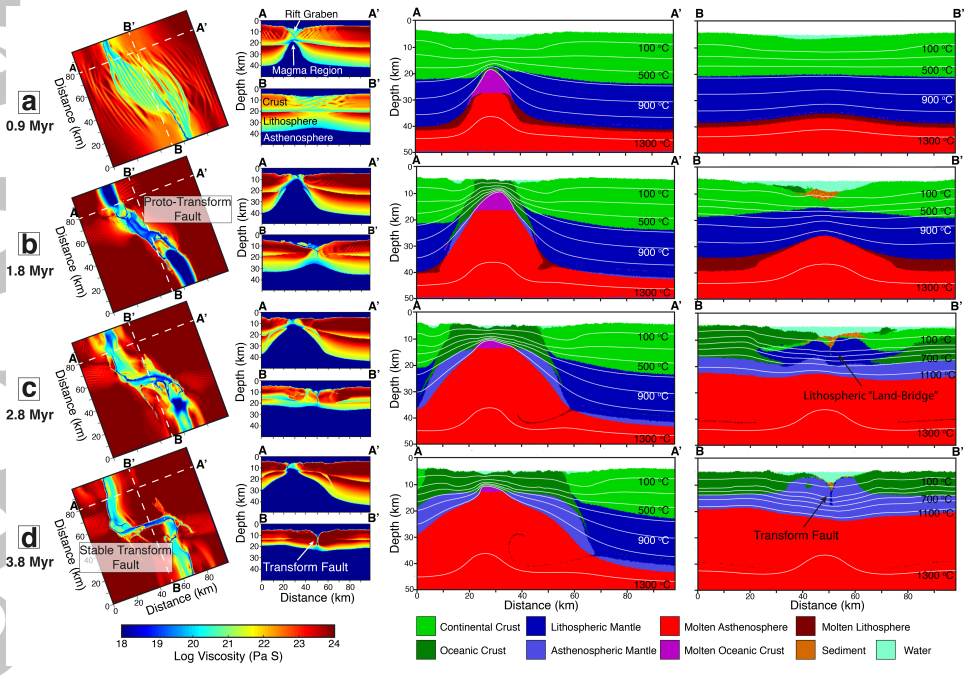

Figure 6. Viscosity variation and pseudo-geological cross-sections within the numerical model of the Giulietti Plain, Northern Afar. Time steps refer to time after model initiation. The viscosity plots clearly show an evolution from broadly distributed deformation in **(a)** followed by the development of the proto-transform fault **(b)**. The proto-transform fault rotates anti-clockwise **(c)** and subsequently evolves to a stable, spreading parallel transform fault **(d)**. Pseudo-geological cross sections show the thinning of the continental crust and accretion of new crustal material. Continental lithosphere is present in the model up until 3.8 Myr, after the formation of a stable transform fault.

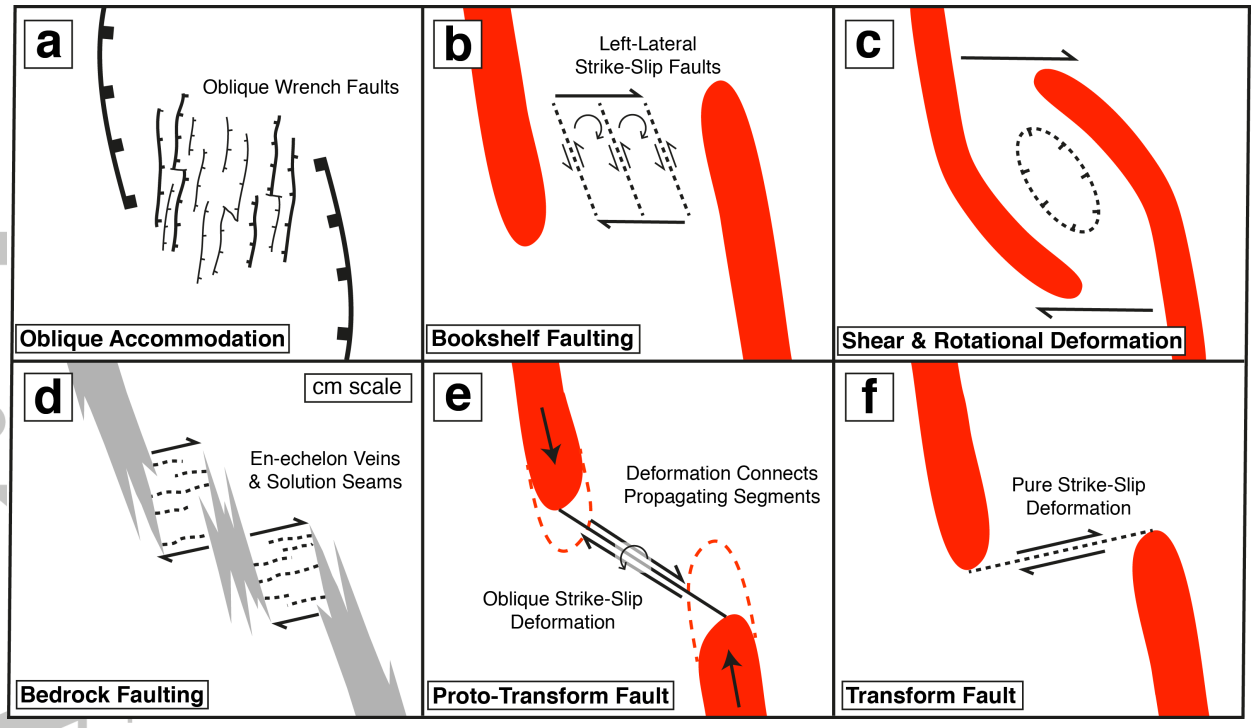

Figure 7. **a)** Extensional transfer observed in early-stage continental rifting. Extension is focused along half-graben structures and transferred through a region of complex, oblique faults (Rosendahl, 1987 ; Bosworth et al., 1986 ; Ebinger, 1989 ; Corti, 2008). **b)** Bookshelf faulting accommodates transfer of extension between between overlapping oceanic spreading segments (Green et al., 2014). **c)** Extension is transferred between overlapping spreading centres through a region of rotational deformation (Macdonald & Fox, 1983 ; Tyler et al., 2007). **d)** Centimetre scale faulting observed in bedrock that accommodates extensional transfer between microcracks (Willemse et al., 1997). **e)** Extensional transfer through a proto-transform fault, observed in young seafloor spreading segments (Taylor et al., 2009) and proposed here for Northern Afar. The proto-transform fault links propagating magmatic segments and rotates anti-clockwise as the segments propagate. **f)** Ridge-perpendicular, spreading parallel oceanic transform faults which are characteristic of ocean ridges (Macdonald et al., 1988).

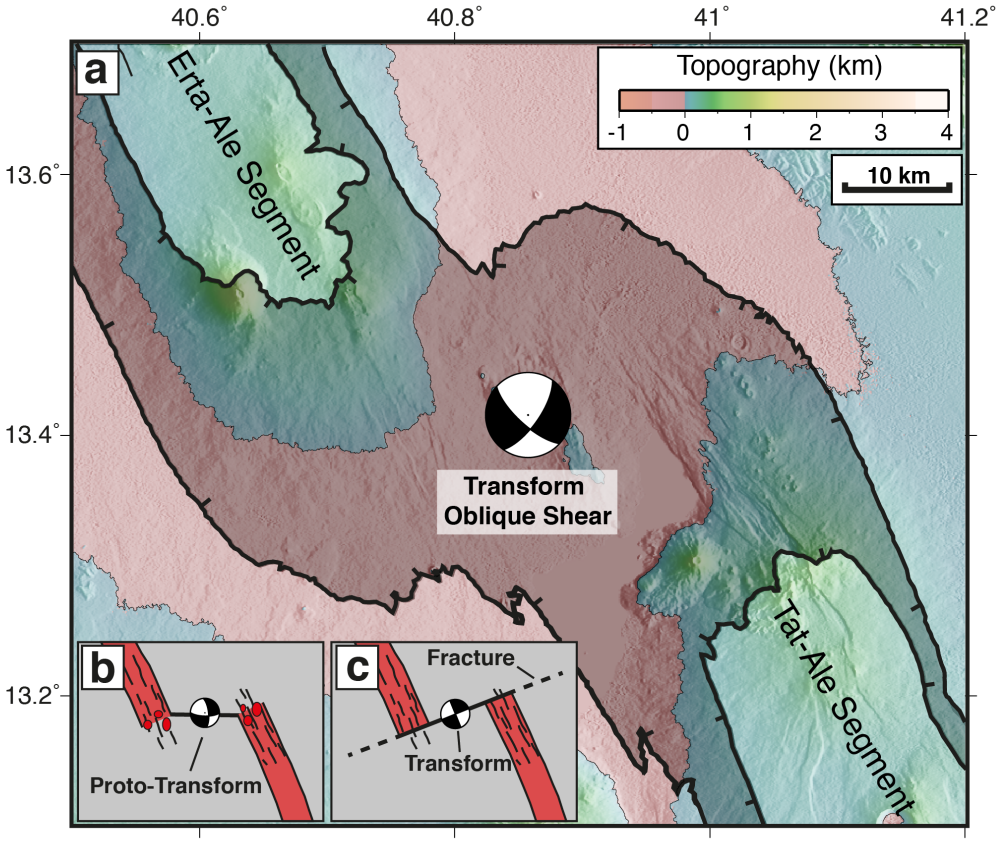

Figure 8. **a)** Topography taken from the numerical model at 1.8 Myr (shaded below sea-level, light above sea- level) overlain on topography from the Giulietti Plain (pink below sea-level) shows good agreement in the location of topographic highs and lows. The oblique, strike-slip faults that are observed in the Giulietti Plain are caused by the transtensional proto-transform fault, as predicted by the numerical model. Modelling further predicts that the proto-transform fault will rotate in an anti-clockwise sense as volcanic segments propagate towards each other **(b)**. The anti-clockwise rotation of the proto-transform fault results in the observed rotation of surface faulting in the Giulietti Plain. The proto-transform fault then develops into a spreading parallel transform fault **(c)**, with pure strike-slip motion. This is then a stable and persistent feature such as transform faults observed at mid-ocean ridges worldwide.